Three-dimensional axon morphologies of individual layer 5 neurons indicate cell type-specific intracortical pathways for whisker motion and touch

Marcel Oberlaender[a,1], Zimbo S. R. M. Boudewijns[b], Tatjana Kleele[c], Huibert D. Mansvelder[b], Bert Sakmann[a,1], and Christiaan P. J. de Kock[b,1]

[a]Digital Neuroanatomy, Max Planck Florida Institute, Jupiter, FL 33458-2906; [b]Center for Neurogenomics and Cognitive Research, Neuroscience Campus Amsterdam, Vrije Universiteit Amsterdam, NL-1087 HV, Amsterdam, The Netherlands; and [c]Institute of Neuroscience, Technical University Munich, D-80802 Munich, Germany

Contributed by Bert Sakmann, January 19, 2011 (sent for review November 20, 2010)

The cortical output layer 5 contains two excitatory cell types, slender- and thick-tufted neurons. In rat vibrissal cortex, slender-tufted neurons carry motion and phase information during active whisking, but remain inactive after passive whisker touch. In contrast, thick-tufted neurons reliably increase spiking preferably after passive touch. By reconstructing the 3D patterns of intracortical axon projections from individual slender- and thick-tufted neurons, filled in vivo with biocytin, we were able to identify cell type-specific intracortical circuits that may encode whisker motion and touch. Individual slender-tufted neurons showed elaborate and dense innervation of supragranular layers of large portions of the vibrissal area (total length, 86.8 ± 5.5 mm). During active whisking, these long-range projections may modulate and phase-lock the membrane potential of dendrites in layers 2 and 3 to the whisking cycle. Thick-tufted neurons with soma locations intermingling with those of slender-tufted ones display less dense intracortical axon projections (total length, 31.6 ± 14.3 mm) that are primarily confined to infragranular layers. Based on anatomical reconstructions and previous measurements of spiking, we put forward the hypothesis that thick-tufted neurons in rat vibrissal cortex receive input of whisker motion from slender-tufted neurons onto their apical tuft dendrites and input of whisker touch from thalamic neurons onto their basal dendrites. During tactile-driven behavior, such as object location, near-coincident input from these two pathways may result in increased spiking activity of thick-tufted neurons and thus enhanced signaling to their subcortical targets.

axon reconstruction | barrel cortex | dysgranular zone

Based on classification of dendrite morphology, cortical layer 5 (L5) contains two primary excitatory cell types: slender- and thick-tufted neurons (1, 2). These two types are considered the main output neurons of a cortical column (3, 4). Slender- (or thin-) tufted pyramidal neurons project to the striatum and are commonly referred to as corticostriatal neurons. Thick- (or tall-) tufted pyramidal neurons project to the posterior nucleus of the thalamus, brainstem, superior colliculus, and pons (5–7). The two neuron types have been characterized across cortical areas, including somatosensory, visual, auditory, motor, and prefrontal cortices, and therefore represent canonical elements of the cortical microcircuitry (8–18).

We recently showed that slender- and thick-tufted neurons in L5 of vibrissal cortex differentially increase spiking activity depending on the behavioral state (19, 20). The majority of slender-tufted neurons carry phase information upon free-whisking (i.e., self-motion of whiskers). Their modulation depth is highest among all excitatory cell types in vibrissal cortex. During quiet (i.e., nonwhisking) periods or passive whisker deflection (i.e., touch), however, slender-tufted neurons remain relatively inactive. In contrast, thick-tufted neurons are reliably activated upon passive whisker touch, but show almost no increased spiking during free-whisking periods.

The pathways that underlie these differences in context-dependent spiking remain controversial (21, 22), but could at least in part be the result of cell type-specific thalamocortical excitation (23–27). Thick-tufted neurons receive input onto their basal dendrites primarily from excitatory neurons in the ventral posterior medial nucleus of the thalamus (VPM), whereas basal dendrites of slender-tufted neurons are primarily innervated by neurons in the medial division of the posterior thalamic nucleus (POm) (24). By using artificial whisking in anesthetized rats, it was suggested that the POm (i.e., paralemniscal) pathway may carry information on whisker motion, whereas the VPM (i.e., lemniscal) pathway may encode whisker touch (in addition to whisker motion). Thus, cell type- and state-specific spiking in L5 during active somatosensation (28, 29) could be mediated by these two functionally and anatomically segregated thalamocortical pathways (23).

Finally, functional and morphological studies of slender- and thick-tufted neurons indicate that these output neurons also contribute to intracortical circuits (17, 30–33). Here, we reconstructed the entire 3D axon projections in the vibrissal area of individual, in vivo filled slender- and thick-tufted neurons in rat vibrissal cortex by using a semiautomated tracing technique (34). We quantified the cell type-specific 3D innervation patterns with respect to the laminar and columnar architecture of the vibrissal cortex and found highly significant, cell type-specific differences in total axon length and intracortical projection patterns.

Considering that slender- and thick-tufted neurons are primarily involved in processing of signals related to the phase of whisker motion and whisker touch, respectively, our anatomical quantification of their intracortical targets leads to a hypothesis on cell type-specific microcircuits that may encode active whisker motion, passive whisker touch, and object location.

Results

Three-Dimensional Intracortical Projections of L5 Slender-Tufted Pyramidal Neurons. Fig. 1 shows one example of five reconstructed slender-tufted neurons in rat vibrissal cortex (Fig. S1). The 3D neuron morphologies (dendrites and axon) were obtained from individual in vivo preparations and are shown in tangential (Fig. 1*A*) and semicoronal view (Fig. 1*B*), respectively. Originally classified by common dendrite morphology (1), slender-tufted

Author contributions: M.O., B.S., and C.P.J.d.K. designed research; M.O., Z.S.R.M.B., T.K., and C.P.J.d.K. performed research; M.O. designed new analytic tools; M.O., Z.S.R.M.B., H.D.M., B.S., and C.P.J.d.K. analyzed data; and M.O., Z.S.R.M.B., H.D.M., B.S., and C.P.J.d.K. wrote the paper.

The authors declare no conflict of interest.

Freely available online through the PNAS open access option.

[1]To whom correspondence may be addressed. E-mail: marcel.oberlaender@maxplanckflorida.org, bert.sakmann@maxplanckflorida.org, or christiaan.de.kock@cncr.vu.nl.

This article contains supporting information online at www.pnas.org/lookup/suppl/doi:10.1073/pnas.1100647108/-/DCSupplemental.

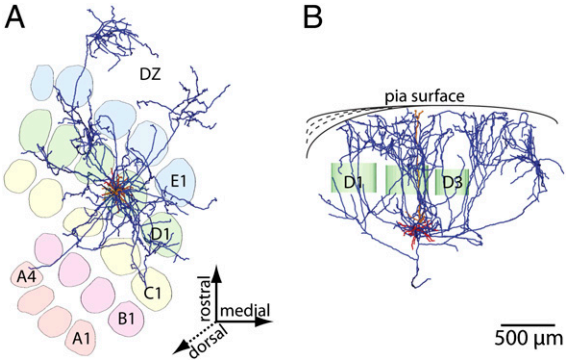

Fig. 1. Three-dimensional reconstructions of in vivo filled slender-tufted pyramidal neuron in L5 of rat vibrissal cortex. (*A*) View on cortical surface (dorsal axis points out of the paper plane). Neuronal processes (axon, blue; basal dendrites, red; apical dendrites, orange) are shown with reference to the barrel field in L4 (letters A–E refer to whisker rows, numbers refer to whiskers within the same row). Note the wide lateral spread and dense innervation of slender-tufted axon into multiple barrel columns surrounding the principal column, which contains the cell's soma. In addition, this neuron displays long-range projections outside the vibrissal area into surrounding higher-order dysgranular cortices (DZ). (*B*) Semicoronal view along whisker row D in *A*. Note that the wide-ranging lateral projections are primarily confined to supragranular layers. Projections in dysgranular cortex originate from a single branch and end in clusters of columnar dimensions.

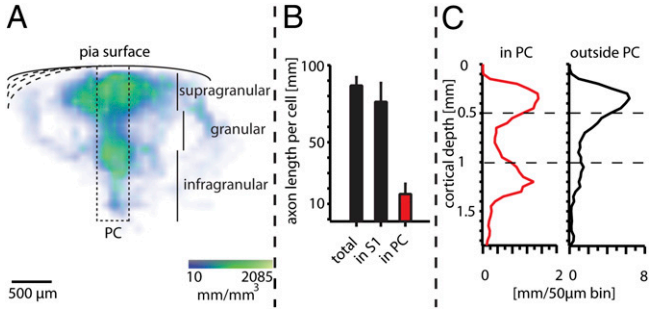

Fig. 2. Quantification of 3D intracortical axon innervation of slender-tufted neurons (I). (*A*) Semicoronal view of 3D axon density of the five neurons shown in Fig. S1. The dashed box renders the approximate dimensions of the respective principal column of each neuron tracing. Note that innervation is not restricted to the principal column (PC), particularly in supragranular layers. (*B*) Most axon is found outside the principal column, or even extends into dysgranular cortices outside the vibrissal area, which cannot be recovered in in vitro preparations. (*C*) Axon length profiles along the vertical column axis. Within the principal column, L5 slender-tufted neurons display two innervation zones: one in supragranular L2/L3 and one in infragranular L5; outside the principal column innervation is largely restricted to supragranular layers, indicating that L5 slender-tufted–L5 projections remain local (i.e., intracolumnar), whereas L5 slender-tufted–L2/L3 projections represent primarily long-range projections (i.e., leaving the principal column).

neurons also share cell type-specific and characteristic intracortical axon projection patterns. First, slender-tufted neurons displayed elaborate and dense lateral projections, innervating large portions of the vibrissal area (Fig. 1*A*). Second, these lateral projections were mostly confined to supragranular layers, whereas granular and infragranular projections remained primarily within the principal column or septa in its immediate vicinity (Fig. 1*B*). Third, two of five neurons displayed significant innervation of higher-order dysgranular cortices adjacent to the vibrissal area (Fig. S1). In the dysgranular zones, projections ended in supragranular depths in clusters of columnar dimensions, originating from a single projecting axon branch, indicating highly specific outgrowth and branching.

To discriminate quantitatively between the short (i.e., columnar) and long-range (i.e., vibrissal area) projections, we measured the total axon length within the principal column, as well as within and outside the vibrissal area (Fig. 2 *A* and *B*). Total axon length of cortical projections from slender-tufted neurons ranged from 79.5 mm to 94.8 mm (86.8 ± 5.5 mm; Fig. 2*B*), of which 16.4 ± 6.7 mm (19%) was confined to the principal column. The majority of axon (59.9 ± 9.7 mm; 69%) was found within the vibrissal area, but outside the principal column, with similar amounts in septa (28.0 ± 7.5 mm) and columns (31.9 ± 7.6 mm). A significant amount of axon (10.6 ± 9.9 mm; 12%) was located in dysgranular zones.

Furthermore, the vertical innervation profiles of axon projections within and outside the principal column displayed significant differences (Figs. 2*C* and 3*A*). Within the principal column, innervation peaks similarly in supragranular layers (6.2 ± 3.6 mm) and infragranular L5 (8.1 ± 2.7 mm). Outside the principal column, innervation is primarily restricted to supragranular depths (43.4 ± 9.7 mm; Fig. 2*C*), exceeding granular (7.1 ± 3.6 mm) and infragranular projections (9.4 ± 3.8 mm) outside the principal column by a factor of three (Fig. 3*B*).

Three-Dimensional Intracortical Projections of L5 Thick-Tufted Pyramidal Neurons. To compare the cell type specificity of intracortical axon projection patterns of L5 output neurons (Table 1), we also reconstructed five axons of individual thick-tufted pyramidal neurons (Fig. S2). Fig. 4 *A* and *B* shows one example neuron in tangential and semicoronal views, respectively. Somata of slender- and thick-tufted neurons were found at overlapping cortical depths of 1,036 ± 46 µm and 1,090 ± 97 µm, respectively. Thus, classification based solely on cortical depth or layer, i.e., into L5A and L5B neurons, was not predictive of morphology. We found that axon branches of thick-tufted neurons were shorter and less complex than those of slender-tufted neurons, with total length ranging from 11.4 mm to 46.5 mm (31.6 ± 14.3 mm; $P < 0.0001$, *t* test; Fig. 5*B*), of which 10.1 ± 6.4 mm (32%) was confined to the principal column. Long-range projections of thick-tufted neurons within the vibrissal area, but outside the principal column, were less elaborate and less dense compared with slender-tufted neurons (18.6 ± 7.5 mm; 59%; $P < 0.0001$, *t* test), and present in equal amounts in septa (9.3 ± 3.9 mm) and columns (9.3 ± 3.8 mm). Furthermore, thick-tufted neurons did not innervate dysgranular zones. Projections to areas outside the vibrissal cortex were restricted to its immediate vicinity and significantly less than slender-tufted ones (2.9 ± 1.8 mm; 9%; $P < 0.001$, *t* test).

With respect to layer-specific innervation profiles, thick-tufted neurons were also significantly different from slender-tufted neurons (Fig. 5*C*). Within the principal column, innervation was

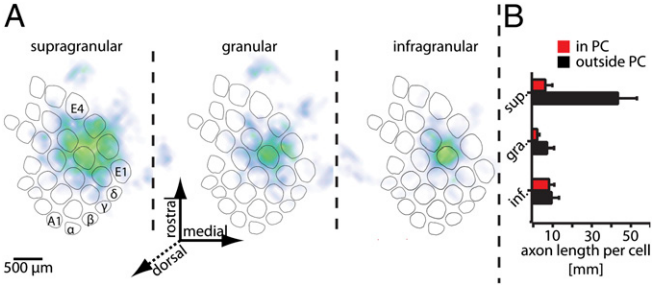

Fig. 3. Quantification of 3D intracortical axon innervation of slender-tufted neurons (II). (*A*) Tangential view of Fig. 2*A* in supragranular, granular, and infragranular layers. Projections from L5 slender-tufted neurons remain largely confined to the principal column in granular and infragranular layers, but innervate almost the entire vibrissal area in supragranular layers. (*B*) Quantification of axon length within and outside the principal column reveals that most axon is found in supragranular layers outside the principal column.

Table 1. Cell type specificity of intracortical axon projection patterns of L5 output neurons

Cortical area	Axon, mm		
	Slender-tufted	Thick-tufted	*P* value (*t* test)
Sensory cortex	86.8 ± 5.5	31.6 ± 14.3	<0.0001
Vibrissal cortex	76.3 ± 12.2	28.7 ± 13.4	<0.001
Supragranular	49.6 ± 10.9	5.1 ± 2.7	<0.0001
Granular	9.2 ± 4.6	4.8 ± 3.0	0.11
Infragranular	17.5 ± 3.8	18.8 ± 8.4	0.76
Columns	48.3 ± 10.5	19.4 ± 9.9	<0.01
Septum	28.0 ± 7.5	9.3 ± 3.9	<0.01
Principal column	16.4 ± 6.7	10.1 ± 6.4	0.17
Supragranular	6.2 ± 3.6	2.1 ± 1.4	0.04
Granular	2.1 ± 1.1	1.4 ± 1.3	0.38
Infragranular	8.1 ± 2.7	6.6 ± 4.1	0.52
Vibrissal cortex without principal column	59.9 ± 9.7	18.6 ± 7.5	<0.0001
Supragranular	43.4 ± 9.7	3.0 ± 1.9	<0.001
Granular	7.1 ± 3.6	3.3 ± 1.8	0.07
Infragranular	9.4 ± 3.8	12.2 ± 4.4	0.31
Columns	31.9 ± 7.6	9.3 ± 3.8	<0.001
Septum	28.0 ± 7.5	9.3 ± 3.9	<0.01
Outside vibrissal cortex	10.6 ± 9.9*	2.9 ± 1.8	<0.001

*Dysgranular zones.

rather homogeneous throughout all layers and reached a maximum in infragranular layers (6.6 ± 4.1 mm). Outside the principal column, most axon was located in deep infragranular layers, where axon branches innervated multiple surrounding columns (12.2 ± 4.4 mm; Fig. 6*B*). Almost no axon was present in supragranular layers (3.0 ± 1.9 mm), marking the most conspicuous difference with respect to slender-tufted neurons ($P < 0.0001$).

Bouton Distributions of L5 Slender- and Thick-Tufted Pyramidal Neurons. To relate the obtained 3D axon projection patterns to innervation densities that may allow speculating on synaptic connectivity, we determined the distance between boutons ($N = 956$) along axons in dysgranular, supragranular, infragranular, and granular regions for slender- and thick-tufted neurons ($n = 4$), respectively. We found swellings that are likely to correspond to en passant and, in some cases, terminaux boutons (35) along all axon branches and in all regions (Fig. S3). The ratio between the two bouton classes was layer- and cell type-specific, which may help to distinguish between these axon types during functional imaging studies (35). However, the small total number of terminaux boutons and the limited resolution of bright-field microscopy prevent us from making absolute statements on bouton statistics.

More importantly, we found that the interbouton distance was similar for slender- and thick-tufted neurons (2.84 ± 1.36 μm vs. 2.90 ± 1.19 μm) and independent of axon location (Fig. S3).

Discussion

The results indicate that slender- and thick-tufted pyramids in L5 have cell type-specific intracortical axon distributions, which differ in (*i*) total axon length, (*ii*) local and long-range projection patterns within different layers of the vibrissal area, and (*iii*) their cortical targets outside the vibrissal area. The axonal length measurements can be directly converted into 3D bouton distributions (as described earlier). In the neocortex, synapses of excitatory neurons are associated with en passant or terminaux boutons (35). Thus, for the present study, axonal length measurements are regarded as predictive of intracortical connectivity (36). As the two neuron types in L5 are differentially involved in whisker motion or passive whisker touch (Fig. S4), the data suggest that cell type-specific intracortical circuits are activated by slender- and thick-tufted neurons depending on the behavioral state, as schematically shown in Fig. 7.

Contribution of Slender-Tufted Neurons to Cortical Signaling During Active Whisking. Spiking in a subset of L5 slender-tufted neurons reliably carries information on position and, more importantly, phase upon active whisker motion (Fig. S4) (20, 37). This information is conveyed subcortically to striatum (38), which is thought to participate in sensory-motor integration to fine-tune whisker movements (5). In addition, our data suggests that information on active whisker motion is relayed via three distinct intracortical pathways (Fig. 7*A*).

The first pathway may target dendrites of L5 neurons within the same principal whisker column, explaining in part the narrow receptive field observed for slender-tufted neurons (19, 39). This column-restricted spread of excitation mediated by slender-tufted neurons within the infragranular layers suggests a column- and therefore whisker-specific corticostriatal output during whisker motion.

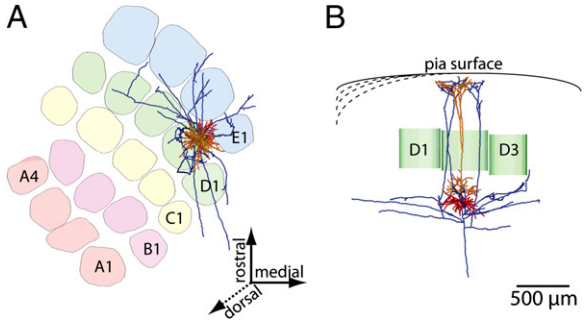

Fig. 4. Three-dimensional reconstructions of in vivo filled thick-tufted pyramidal neuron in L5 of rat vibrissal cortex. (*A*) Tangential view and notation as in Fig. 1*A*. Note that the intracortical axon innervation by thick-tufted cells is far less elaborate compared with slender-tufted neurons. Further, innervation remains largely confined to the principal column and a limited number of surrounding columns in its immediate vicinity. (*B*) Semicoronal view as in Fig. 1*A*. Please note that the horizontal projections to surrounding columns remain primarily confined to infragranular layers, whereas projections to granular and supragranular layers remain within the lateral boundaries of the principal column.

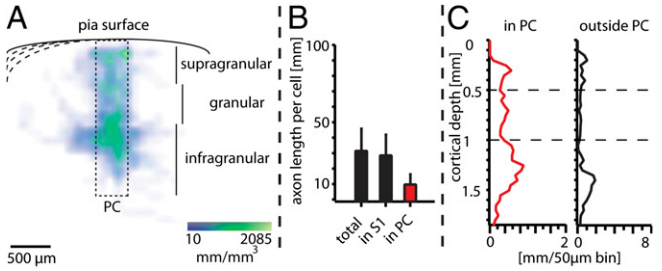

Fig. 5. Quantification of 3D intracortical axon innervation of thick-tufted neurons (I). (*A*) Semicoronal view of 3D axon density of the five neurons shown in Fig. S2. Please note that innervation in granular and supragranular layers respects the lateral borders of the principal column, whereas innervation in infragranular layers extends to surrounding columns. (*B*) Thick-tufted neurons display much less axon compared with slender-tufted neurons (Fig. 2*B*). Whereas the amount of axon is similar for slender-tufted and thick-tufted neurons within the principal column (16.4 ± 6.7 vs. 10.1 ± 6.4; $P = 0.17$), long-range projections are significantly less elaborate for thick-tufted neurons (59.6 ± 9.7 vs. 18.6 ± 7.5; $P < 0.0001$). (*C*) The axon length profile of thick-tufted neurons within the principal column reveals that intracolumnar innervation is almost homogeneous throughout all layers, reaching a peak in infragranular L5 approximately 1,250 µm below the pia surface. The profile outside the principal column shows that long-range projections are confined to infragranular layers.

The second pathway targets dendrites located within supragranular layers of a large portion of the vibrissal area, which primarily contain basal and apical dendrites of L2 and L3 pyramidal neurons, apical tufts of L5 thick-tufted and slender-tufted neurons (24), as well as dendrites from L2 and L3 inhibitory interneurons (40). Axon projections of L5 slender-tufted neurons have been shown to establish functional connections with L2/L3 pyramidal neurons (32, 33). However, as spiking in supragranular layers does not increase significantly upon active whisking (20, 41), the sensory information carried by these intracortical long range projections is likely within fine-scale synaptic activity (42). During active whisking, the membrane potential of L2 and L3 pyramidal neurons may therefore be locked to the phase of individual slender-tufted neurons (41). However, more importantly, slender-tufted projections to supragranular layers may also target the apical tuft dendrites of L5 thick-tufted neurons, present at high density in supragranular layers (24). These long-range L5 slender-tufted projections may then serve to depolarize and phase-lock the membrane potential of apical tuft dendrites of L5 thick-tufted neurons to whisker motion.

The third target population of L5 slender-tufted neurons comprises a previously unknown pathway to supragranular depths of higher-order dysgranular zones adjacent to the vibrissal area. We hypothesize that this direct cortical pathway from vibrissal to dysgranular cortex underlies the activity observed previously in dysgranular zones after stimulation of the whiskers or intervibrissal skin and fur (43–45). Dysgranular zones are thought to participate in multisensory integration of auditory, visual, and somatosensory stimuli (43), rendering L5 slender-tufted neurons as one potential cell type that signals whisker motion and position to higher-order sensory areas in a phase-sensitive way.

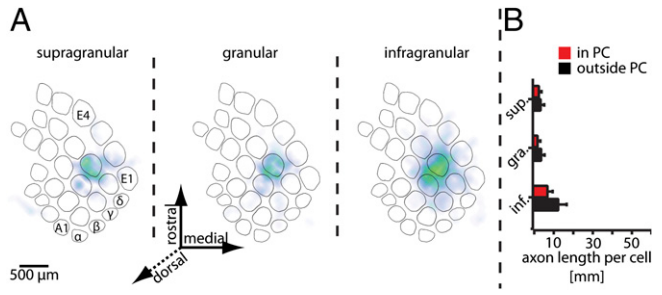

Fig. 6. Quantification of 3D intracortical axon innervation of thick-tufted neurons (II). (*A*) Tangential view of Fig. 5*A* in supragranular, granular, and infragranular layers. Projections of thick-tufted neurons remain almost completely confined to the lateral column boundaries in granular and supragranular layers, but spread to adjacent columns in infragranular layers. (*B*) Quantification of axon length within and outside the principal column reveals that most axon is found in infragranular layers outside the principal column.

Contribution of Thick-Tufted Neurons to Cortical Signaling After Passive Whisker Touch. L5 thick-tufted neurons reliably increase spiking after passive whisker touch (19). This increase may be primarily caused by thalamocortical input to basal dendrites from VPM neurons via the lemniscal pathway (23–26, 39, 46).

Our data suggest that thick-tufted neurons may contribute significantly less to signaling via intracortical pathways (Fig. 7*B*) than slender-tufted neurons. Axon projections into granular and supragranular layers are sparser and mostly confined to the principal whisker column, suggesting an almost column-restricted spread of intracortical excitation. However, thick-tufted neurons project more densely to infragranular layers of the principal and surrounding columns, explaining in part the broad sub- and suprathreshold receptive fields of thick-tufted neurons (19, 39, 47) and suggesting that output to subcortical targets from thick-tufted neurons may be less column- and therefore whisker-specific than that from slender-tufted neurons.

Thick-Tufted Neurons May Function as Coincidence Detectors During Object Location. In vitro, L5 thick-tufted neurons have been shown to act as coincidence detectors when basal and apical trees are simultaneously depolarized within a critical time window (48–50). Input to the basal dendrites evokes action potentials back-propagating into the apical dendrite, which, when coinciding with depolarization from the apical tuft, results in an increased

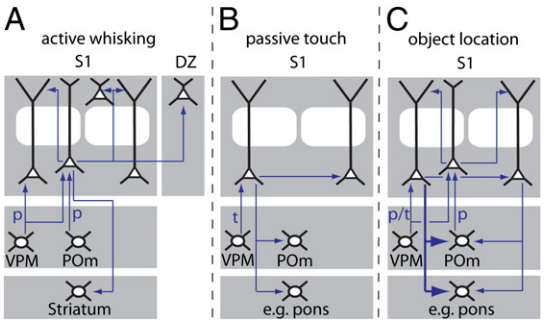

Fig. 7. Cell type-specific microcircuits in L5 are involved during different behavioral states. (*A*) During active whisking, slender-tufted neurons display spiking activity that carries phase information (p). Because of their intracortical axon projection pattern, slender-tufted neurons from a single column convey this information (*i*) via local circuits to L5 neurons within the principal column (not shown), yielding whisker-specific output of slender-tufted neurons to the striatum; and (*ii*) via long-range circuits to supragranular layers of the entire vibrissal area and adjacent dysgranular zones, diminishing whisker specificity in supragranular layers. (*B*) During passive whisker touch, thick-tufted neurons display the highest increase in spiking activity in vibrissal cortex, primarily caused by thalamocortical input from VPM (t). Because of their 3D intracortical axon pattern, thick-tufted neurons from a single cortical column convey information of whisker touch (*i*) via local circuits to all layers within the principal column (not shown), (*ii*) via long-range circuits to L5 of surrounding columns, and (*iii*) to subcortical targets (e.g., POm and pons). (*C*) Object location during active whisker motion may be encoded by simultaneous input from slender-tufted neurons to apical tufts and from VPM to basal dendrites of L5 thick-tufted neurons, causing increased spiking activity (bold arrow) and enhanced output to subcortical targets (e.g., corticothalamic feedback to POm).

number of spikes and evokes bursts of somatic and axonal action potentials (49, 51).

We suggest that, in vivo, L5 thick-tufted neurons of vibrissal cortex are activated under two different conditions. First, excitatory input from VPM to basal dendrites drives L5 thick-tufted neurons to spiking threshold after passive whisker touch and results in single or short trains of spikes (52). Second, near-simultaneous activation of L5 slender-tufted and VPM pathways during sensory-motor behavioral paradigms, such as object location during active whisking, may coincidentally depolarize basal and apical dendrites of L5 thick-tufted neurons and cause increased (i.e., burst) activity (Fig. 7*C*) (37, 53), which is then conveyed to intra- and subcortical targets.

We put forward the hypothesis that individual L5 slender-tufted neurons serve primarily as intracortical hubs of cell-specific information on whisker motion and phase. They potentially modulate the membrane potential of all dendrites in supragranular layers (including those of inhibitory neurons) within large portions of the vibrissal area according to their phase and lock them to specific parts of the whisking cycle. This cell-specific phase-locking may facilitate encoding of object location, which comprises simultaneous, unspecific input on whisker touch from VPM neurons to the basal dendrites and specific input on whisker phase from L5 slender-tufted neurons to the apical tufts of L5 thick-tufted neurons (Fig. 7*C*).

Additional Pathways for Integration of Whisker Motion and Active Touch. Other intra- and thalamocortical mechanisms for integration of whisker motion and touch may exist in parallel to the pathways described here. L5 slender-tufted neurons may also function as coincidence detectors when lemniscal input from L4 (30, 54) and paralemniscal input occur simultaneously (14). However, somatic action potentials only back-propagate into the apical dendrite for short distances during spiking frequencies that are observed in vivo (55). It seems therefore more likely that L5 slender-tufted neurons integrate input on whisker motion and touch at the soma (37, 56), but coincidence detection via near-simultaneous input to basal and apical tuft dendrites is less likely to occur.

Furthermore, direct innervation from POm onto apical dendrites of L5 thick-tufted neurons could serve in a similar way as the input from slender-tufted neurons suggested here (24, 57). Another possibility for simultaneous input on whisker motion and touch could involve direct innervation from the primary motor cortex (6, 25) onto apical dendrites of L5 thick-tufted neurons.

Conclusion

Considering that slender-tufted neurons predominantly carry phase information during active whisker motion and that thick-tufted neurons are preferentially activated upon passive whisker touch, we argue that the pathways we described here are realistic candidates for encoding object location. The emergence of cell type-specific genetic labels for slender- and thick-tufted neurons (38) sets the stage to specifically manipulate the activity of slender- and/or thick-tufted neurons, which may ultimately prove or disprove the functional contributions of the pathways described here during whisker-mediated behavior.

Methods

Juxtasomal Labeling with Biocytin. Recordings from urethane anesthetized Wistar rats (postnatal day 28 ± 1) were made as described previously (19). Cytochrome C oxidase staining was used to label barrel contours in L4 (58). The recorded neurons were labeled with the chromogen 3,3′-diaminobenzidine tetrahydrochloride (59) by using the avidin–biotin–peroxidase method. Selection criteria for reconstructions included adequate labeling, sufficient cytochrome C signal to reconstruct the barrel/septum pattern, and reliable serial reconstruction of long-range axon branches (60).

Three-Dimensional Semiautomated Reconstruction of Neuron Morphology. Neuron tracings were performed on 100-μm-thick Vibratome sections cut approximately tangential to the D2 barrel column. Ranging from the pia surface to the white matter, 20 sections were reconstructed per neuron. 3,3′-Diaminobenzidine tetrahydrochloride-stained neuronal branches were detected and traced by using a previously described automated pipeline (34) and optimized mosaic/optical sectioning microscopy (61). In cases in which neuronal branches reached the borders of the imaged volume, additional image stacks were taken at adjacent areas. Manual postprocessing of individual sections (62), as well as automated alignment of reconstructed branches across sections (63), were performed by using a custom-designed 3D editing environment based on Amira visualization software (64). Pia and barrel outlines were manually drawn on low-resolution images and added to the tracings in Neurolucida software (MicroBrightfield).

Data Analysis. All neurons were transformed into a standardized coordinate system having its origin at the center of the L4 barrel containing the neuron's apical dendrite ("principal barrel"). The *z* axis pointed dorsally, parallel to the vertical barrel axis; the *x* axis laterally toward the center of the first neighboring barrel within the same whisker row. Analysis of these standardized neurons was performed in Amira software with use of custom-written tools.

Axon length per individual column was determined by extrapolating the respective barrel contours along the vertical axis toward the pia and white matter. Axon structures that are not contained within any column were counted as septal projections. Supragranular, granular, and infragranular projections were measured for each column individually, as barrel size or thickness of the cortex may vary between columns.

Average axon density distributions were determined by aligning all axons to the D2 column, but preserving vertical and lateral position of the soma as well as orientation with respect to the barrel center. The maximal 3D bounding box surrounding all axons was subdivided into 100-μm voxels. Density is presented as axon length per such voxel.

Average interbouton distances were obtained manually by using a transmitted light bright-field microscope equipped with a 100× oil immersion objective (numerical aperture, 1.4) and Neurolucida software. Preferentially, horizontally projecting axons were chosen for analysis. Interbouton distances were determined by using the Quick Measure tool in Neurolucida for samples from two slender- and thick-tufted neurons, respectively.

Data are presented as mean ± SD and GraphPad Instat 3 software was used for statistical analysis. Significance level was set at $P < 0.05$.

ACKNOWLEDGMENTS. We thank Andrea Weber and Sebastiano Bellanca for Neurolucida reconstructions during initial stages of the project, Vincent J. Dercksen for implementing analysis tools in Amira; Marlies Kaiser, Ellen Stier, and Brendan Lodder for excellent technical support; Robert Egger for his help on the bouton counts; and Hanno-Sebastian Meyer and Jason Christie for fruitful discussions. This work was supported by the Max-Planck Society, the Center for Neurogenomics and Cognitive Research at Vrije Universiteit Amsterdam, and a Veni Grant from The Netherlands Organization for Scientific Research (to C.P.J.d.K.).

1. Hallman LE, Schofield BR, Lin CS (1988) Dendritic morphology and axon collaterals of corticotectal, corticopontine, and callosal neurons in layer V of primary visual cortex of the hooded rat. *J Comp Neurol* 272:149–160.
2. Larkman A, Mason A (1990) Correlations between morphology and electrophysiology of pyramidal neurons in slices of rat visual cortex. I. Establishment of cell classes. *J Neurosci* 10:1407–1414.
3. Jones EG (1984) *Cerebral cortex*. Laminar Distribution of Cortical Efferent Cells, eds Peters A, Jones EG (Plenum, New York), pp 521–553.
4. Meyer HS, et al. (2010) Number and laminar distribution of neurons in a thalamocortical projection column of rat vibrissal cortex. *Cereb Cortex* 20:2277–2286.
5. Alloway KD (2008) Information processing streams in rodent barrel cortex: the differential functions of barrel and septal circuits. *Cereb Cortex* 18:979–989.
6. Aronoff R, et al. (2010) Long-range connectivity of mouse primary somatosensory barrel cortex. *Eur J Neurosci* 31:2221–2233.
7. Groh A, de Kock CP, Wimmer VC, Sakmann B, Kuner T (2008) Driver or coincidence detector: Modal switch of a corticothalamic giant synapse controlled by spontaneous activity and short-term depression. *J Neurosci* 28:9652–9663.
8. Binzegger T, Douglas RJ, Martin KA (2004) A quantitative map of the circuit of cat primary visual cortex. *J Neurosci* 24:8441–8453.
9. Sakata S, Harris KD (2009) Laminar structure of spontaneous and sensory-evoked population activity in auditory cortex. *Neuron* 64:404–418.
10. Ojima H, Honda CN, Jones EG (1992) Characteristics of intracellularly injected infragranular pyramidal neurons in cat primary auditory cortex. *Cereb Cortex* 2: 197–216.

11. Brown SP, Hestrin S (2009) Intracortical circuits of pyramidal neurons reflect their long-range axonal targets. *Nature* 457:1133–1136.
12. Morishima M, Kawaguchi Y (2006) Recurrent connection patterns of corticostriatal pyramidal cells in frontal cortex. *J Neurosci* 26:4394–4405.
13. Brecht M, Schneider M, Sakmann B, Margrie TW (2004) Whisker movements evoked by stimulation of single pyramidal cells in rat motor cortex. *Nature* 427:704–710.
14. Schubert D, Kotter R, Staiger JF (2007) Mapping functional connectivity in barrel-related columns reveals layer- and cell type-specific microcircuits. *Brain Struct Funct* 212:107–119.
15. Gao WJ, Zheng ZH (2004) Target-specific differences in somatodendritic morphology of layer V pyramidal neurons in rat motor cortex. *J Comp Neurol* 476:174–185.
16. Hübener M, Schwarz C, Bolz J (1990) Morphological types of projection neurons in layer 5 of cat visual cortex. *J Comp Neurol* 301:655–674.
17. Larsen DD, Wickersham IR, Callaway EM (2007) Retrograde tracing with recombinant rabies virus reveals correlations between projection targets and dendritic architecture in layer 5 of mouse barrel cortex. *Front Neural Circuits* 1:5.
18. Martinez LM, et al. (2005) Receptive field structure varies with layer in the primary visual cortex. *Nat Neurosci* 8:372–379.
19. de Kock CP, Bruno RM, Spors H, Sakmann B (2007) Layer- and cell-type-specific suprathreshold stimulus representation in rat primary somatosensory cortex. *J Physiol* 581:139–154.
20. de Kock CP, Sakmann B (2009) Spiking in primary somatosensory cortex during natural whisking in awake head-restrained rats is cell-type specific. *Proc Natl Acad Sci USA* 106:16446–16450.
21. Ahissar E, Golomb D, Haidarliu S, Sosnik R, Yu C (2008) Latency coding in POm: Importance of parametric regimes. *J Neurophysiol* 100:1152–1154.
22. Masri R, Bezdudnaya T, Trageser JC, Keller A (2008) Encoding of stimulus frequency and sensor motion in the posterior medial thalamic nucleus. *J Neurophysiol* 100: 681–689.
23. Yu C, Derdikman D, Haidarliu S, Ahissar E (2006) Parallel thalamic pathways for whisking and touch signals in the rat. *PLoS Biol* 4:e124.
24. Meyer HS, et al. (2010) Cell type-specific thalamic innervation in a column of rat vibrissal cortex. *Cereb Cortex* 20:2287–2303.
25. Petreanu L, Mao T, Sternson SM, Svoboda K (2009) The subcellular organization of neocortical excitatory connections. *Nature* 457:1142–1145.
26. Bureau I, von Saint Paul F, Svoboda K (2006) Interdigitated paralemniscal and lemniscal pathways in the mouse barrel cortex. *PLoS Biol* 4:e382.
27. Urbain N, Deschênes M (2007) A new thalamic pathway of vibrissal information modulated by the motor cortex. *J Neurosci* 27:12407–12412.
28. Knutsen PM, Pietr M, Ahissar E (2006) Haptic object localization in the vibrissal system: Behavior and performance. *J Neurosci* 26:8451–8464.
29. Mehta SB, Whitmer D, Figueroa R, Williams BA, Kleinfeld D (2007) Active spatial perception in the vibrissa scanning sensorimotor system. *PLoS Biol* 5:e15.
30. Schubert D, Kötter R, Luhmann HJ, Staiger JF (2006) Morphology, electrophysiology and functional input connectivity of pyramidal neurons characterizes a genuine layer va in the primary somatosensory cortex. *Cereb Cortex* 16:223–236.
31. Schubert D, et al. (2001) Layer-specific intracolumnar and transcolumnar functional connectivity of layer V pyramidal cells in rat barrel cortex. *J Neurosci* 21:3580–3592.
32. Shepherd GM, Stepanyants A, Bureau I, Chklovskii D, Svoboda K (2005) Geometric and functional organization of cortical circuits. *Nat Neurosci* 8:782–790.
33. Shepherd GM, Svoboda K (2005) Laminar and columnar organization of ascending excitatory projections to layer 2/3 pyramidal neurons in rat barrel cortex. *J Neurosci* 25:5670–5679.
34. Oberlaender M, Bruno RM, Sakmann B, Broser PJ (2007) Transmitted light brightfield mosaic microscopy for three-dimensional tracing of single neuron morphology. *J Biomed Opt* 12:064029.
35. De Paola V, et al. (2006) Cell type-specific structural plasticity of axonal branches and boutons in the adult neocortex. *Neuron* 49:861–875.
36. Peters A (1979) Thalamic input to the cerebral cortex. *Trends Neurosci* 2:1183–1185.
37. Curtis JC, Kleinfeld D (2009) Phase-to-rate transformations encode touch in cortical neurons of a scanning sensorimotor system. *Nat Neurosci* 12:492–501.
38. Groh A, et al. (2010) Cell-type specific properties of pyramidal neurons in neocortex underlying a layout that is modifiable depending on the cortical area. *Cereb Cortex* 20:826–836.
39. Manns ID, Sakmann B, Brecht M (2004) Sub- and suprathreshold receptive field properties of pyramidal neurones in layers 5A and 5B of rat somatosensory barrel cortex. *J Physiol* 556:601–622.
40. Helmstaedter M, Sakmann B, Feldmeyer D (2008) The relation between dendritic geometry, electrical excitability, and axonal projections of l2/3 interneurons in rat barrel cortex. *Cereb Cortex* 19:938–950.
41. Crochet S, Petersen CC (2006) Correlating whisker behavior with membrane potential in barrel cortex of awake mice. *Nat Neurosci* 9:608–610.
42. Alenda A, Molano-Mazón M, Panzeri S, Maravall M (2010) Sensory input drives multiple intracellular information streams in somatosensory cortex. *J Neurosci* 30: 10872–10884.
43. Brett-Green BA, Chen-Bee CH, Frostig RD (2001) Comparing the functional representations of central and border whiskers in rat primary somatosensory cortex. *J Neurosci* 21:9944–9954.
44. Takashima I, Kajiwara R, Iijima T (2005) Voltage-sensitive dye imaging of intervibrissal fur-evoked activity in the rat somatosensory cortex. *Neurosci Lett* 381:258–263.
45. Nussbaumer JC, Van der Loos H (1985) An electrophysiological and anatomical study of projections to the mouse cortical barrelfield and its surroundings. *J Neurophysiol* 53:686–698.
46. Wimmer VC, Bruno RM, de Kock CP, Kuner T, Sakmann B (2010) Dimensions of a projection column and architecture of VPM and POm axons in rat vibrissal cortex. *Cereb Cortex* 20:2265–2276.
47. Ito M (1992) Simultaneous visualization of cortical barrels and horseradish peroxidase-injected layer 5b vibrissa neurones in the rat. *J Physiol* 454:247–265.
48. Schaefer AT, Larkum ME, Sakmann B, Roth A (2003) Coincidence detection in pyramidal neurons is tuned by their dendritic branching pattern. *J Neurophysiol* 89: 3143–3154.
49. Larkum ME, Zhu JJ, Sakmann B (1999) A new cellular mechanism for coupling inputs arriving at different cortical layers. *Nature* 398:338–341.
50. Spruston N (2008) Pyramidal neurons: dendritic structure and synaptic integration. *Nat Rev Neurosci* 9:206–221.
51. Larkum ME, Zhu JJ, Sakmann B (2001) Dendritic mechanisms underlying the coupling of the dendritic with the axonal action potential initiation zone of adult rat layer 5 pyramidal neurons. *J Physiol* 533:447–466.
52. de Kock CP, Sakmann B (2008) High frequency action potential bursts (>or= 100 Hz) in L2/3 and L5B thick tufted neurons in anaesthetized and awake rat primary somatosensory cortex. *J Physiol* 586:3353–3364.
53. O'Connor DH, Peron SP, Huber D, Svoboda K (2010) Neural activity in barrel cortex underlying vibrissa-based object localization in mice. *Neuron* 67:1048–1061.
54. Feldmeyer D, Roth A, Sakmann B (2005) Monosynaptic connections between pairs of spiny stellate cells in layer 4 and pyramidal cells in layer 5A indicate that lemniscal and paralemniscal afferent pathways converge in the infragranular somatosensory cortex. *J Neurosci* 25:3423–3431.
55. Grewe BF, Bonnan A, Frick A (2010) Back-propagation of physiological action potential output in dendrites of slender-tufted L5A pyramidal neurons. *Front Cell Neurosci* 4:13.
56. O'Connor DH, et al. (2010) Vibrissa-based object localization in head-fixed mice. *J Neurosci* 30:1947–1967.
57. Zhu Y, Zhu JJ (2004) Rapid arrival and integration of ascending sensory information in layer 1 nonpyramidal neurons and tuft dendrites of layer 5 pyramidal neurons of the neocortex. *J Neurosci* 24:1272–1279.
58. Horikawa K, Armstrong WE (1988) A versatile means of intracellular labeling: Injection of biocytin and its detection with avidin conjugates. *J Neurosci Methods* 25:1–11.
59. Wong-Riley M (1979) Changes in the visual system of monocularly sutured or enucleated cats demonstrable with cytochrome oxidase histochemistry. *Brain Res* 171:11–28.
60. Kaspirzhny AV, Gogan P, Horcholle-Bossavit G, Tyc-Dumont S (2002) Neuronal morphology data bases: morphological noise and assessment of data quality. *Network* 13:357–380.
61. Oberlaender M, Broser PJ, Sakmann B, Hippler S (2009) Shack-Hartmann wave front measurements in cortical tissue for deconvolution of large three-dimensional mosaic transmitted light brightfield micrographs. *J Microsc* 233:275–289.
62. Dercksen VJ, Oberlaender M, Sakmann B, Hege HC (2010) Interactive visualization – a key prerequisite for reconstruction of anatomically realistic neural networks. *Proceedings of the 2nd Annual Workshop on Visualization in Medicine and Life Sciences (VMLS 09).* (Springer-Verlag, Berlin), in press.
63. Dercksen VJ, et al. (2009) Automatic alignment of stacks of filament data. *IEEE International Symposium on Biomedical Imaging: From Nano to Macro (ISBI)* (IEEE Press, Boston), pp 971–974.
64. Stalling D, Westerhoff M, Hege HC (2005) Amira: A Highly Interactive System for Visual Data Analysis. *The Visualization Handbook*, eds Hansen CD, Johnson CR (Elsevier, Amsterdam), pp 749–767.